Journal of Nanobiotechnology

RESEARCH Open Access

AG73-GelMA/AlgMA hydrogels provide a stable microenvironment for the generation of pancreatic progenitor organoids

Jian Wan[1,2†], Yang Xu[1,2†], Tianmu Qi[4†], Xiaoxia Xue[5], Yuxi Li[4], Minjie Huang[4], Yuchen Guo[4], Qingsong Guo[1,2*], Yuhua Lu[1,2*] and Yan Huang[1,2,3*]

Abstract

Patient specific induced pluripotent stem cells (iPSCs) derived β cells represent an effective means for disease modeling and autologous diabetes cell replacement therapy. In this study, an AG73-5%gelatin methacryloyl (GelMA) /2% alginate methacrylate (AlgMA) hydrogel was employed to generate pancreatic progenitor (PP) organoids and improve stem cell-derived β (SC-β) cell differentiation protocol. The laminin-derived homolog AG73, which mimics certain cell–matrix interactions, facilitates AKT signaling pathway activation to promote PDX1$^+$/NKX6.1$^+$ PP organoid formation and effectively modulates subsequent epithelial–mesenchymal transition (EMT) in the endocrine lineage. The 5%GelMA/2%AlgMA hydrogel mimics the physiological stiffness of the pancreas, providing the optimal mechanical stress and spatial structure for PP organoid differentiation. The Syndecan-4 (SDC4)-ITGAV complex plays a pivotal role in the early stages of pancreatic development by facilitating the formation of SOX9$^+$/PDX1$^+$ bipotent PPs. Our findings demonstrate that AG73-GelMA/AlgMA hydrogel-derived SC-β cells exhibit enhanced insulin secretion and accelerated hyperglycemia reversal in vivo. This study presents a cost-effective, stable, and efficient alternative for the comprehensive 3D culture of SC-β cells in vitro by mitigating the uncertainties associated with conventional culture methods.

Introduction

Currently, islet transplantation is the most promising therapeutic approach for reversin the natural progression of diabetes in patients with unstable diabetes or severe complications [1]. However, its clinical application is significantly impeded by the relative shortage of donors. In recent years, remarkable advancements have been made in using stem cell-derived β (SC-β) cell transplantation to treat diabetes, and several approaches have progressed to the clinical trial stage [2, 3]. Notably, the unlimited proliferation and differentiation potential of stem cells theoretically addresses the issue of β-cell scarcity. The current focus and challenge lies in regulating the generation of pancreatic-specific subpopulation cells and enhancing SC-β cell production while minimizing superfluous cells,

†Jian Wan, Yang Xu and Tianmu Qi contributed equally to this work.

*Correspondence:
Qingsong Guo
ntgglj@163.com
Yuhua Lu
lyh76@126.com
Yan Huang
nthy1210@ntu.edu.cn

Full list of author information is available at the end of the article

Graphical Abstract

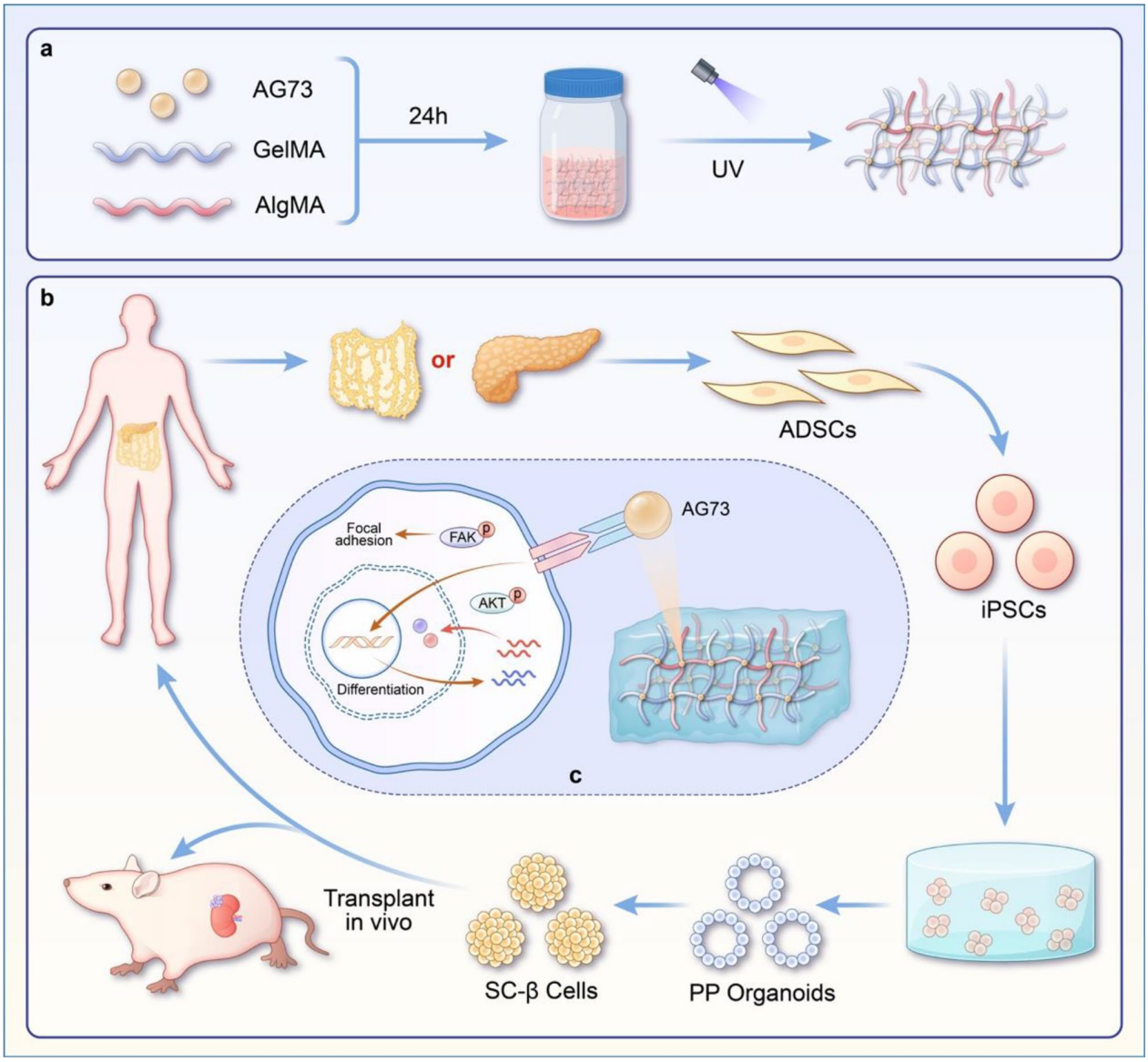

Keywords GelMA/AlgMA hydrogel, Induced pluripotent stem cells, Organoids, Differentiation, Diabetes

particularly undifferentiated cells with tumorigenicity [4]. Within the established multistep pancreatic development differentiation system, it is crucial to generate pancreatic progenitor cells (PPs) with an endocrine lineage differentiation trajectory, which would ultimately lead to functional β-cell differentiation [5]. For example, $PDX1^+$ and $NKX6.1^+$ PPs are regarded as progenitor cells with a monohormonal lineage that determines the generation of β-cells [6]. However, conventional differentiation models overlook how the in vivo extracellular matrix (ECM) microenvironment affects cell differentiation, resulting in nonphysiological responses and reduced differentiation efficiency.

In recent years, engineered defined hydrogels have gained popularity among researchers because of their ability to accurately replicate the ECM microenvironment, substrate mechanics, and cell–ligand interactions for stem cell cultivation and in vitro differentiation [7]. Moreover, defined hydrogels constructed with specific peptides or proteins can precisely control stem cell behavior and promote their directional differentiation. Kong et al. utilized a Supragel hydrogel to provide a

supporting stiffness of ~1.5 kPa, which promoted more efficient human induced pluripotent stem cells (hiPSCs) differentiation into endodermal and subsequently, insulin-secreting cells [8]. Several identified peptides, such as RGD, AG73, IKVAV, and GFOGER, have been adopted in research with promising outcomes [9]. In our previous study, we identified the LAMA2 hydrogel as a highly efficacious biomimetic carrier that promotes the formation and maturation of the pancreatic endocrine lineage [10]. We also found that the self-differentiation and maturation of insulin-producing cells (IPCs) could be promoted only by altering the ECM [11]. The manipulation of physical ECM cues to induce cell differentiation has recently gained increasing attention from researchers [12]. Syndecan-4 (SDC4), a mechanical cue-related protein identified by data-independent acquisition (DIA) sequencing, attracted our attention. SDC4 serves as a pivotal cell surface mechanical signal transduction coreceptor, facilitating the formation of focal adhesions and stress fibers within cells through its interactions with integrins. These interactions activate the integrins, enabling the transmission of ECM signals to the nucleus [13]. The peptide AG73 effectively allows cells to receive ECM stimulation by binding to the SDC4 domain through ligand–receptor interactions [14].

Significant advancements in the fields of biomaterials and bioengineering have led to the emergence of a new era known as "organoid customization" [15]. Defined hydrogels offer broader opportunities to support the establishment of organoids because of their finely tuned biochemical and biophysical properties [16]. These organoids exhibit remarkable tissue heterogeneity that closely mimics that of native organs. For example, neural organoids constructed from polyethylene glycol (PEG) hydrogels exhibit increased neuronal diversity, reduced tissue heterogeneity, and potential physiological functionality [17]. The establishment of pancreatic organoids has faced challenges, such as discrepancies in cell type and proportion within the structure, over decades of development. Additionally, pancreatic organoid cultures show significant variations between batches and individuals [18]. Therefore, developing a stable and efficient system for pancreatic differentiation holds great significance in achieving the goals in the biomanufacture of pancreatic islets.

In this project, tissue engineering and proteomics were integrated to construct an AG73 biomimetic hydrogel for reconstruction of the pancreatic developmental microenvironment, with the aim of obtaining high-efficiency PPs in vitro and stable SC-β cells for diabetes transplantation therapy. To demonstrate the clinical applicability of this investigation, patient-derived iPSCs were acquired to generate PP organoids for subsequent differentiation into SC-β cells. The findings here demonstrate that the AG73 biomimetic hydrogel can enhance the generation of $PDX1^+/NKX6.1^+$ PP organoids and improve the differentiation efficiency and function of SC-β cells. Additionally, mechanical signal transduction mediated by AG73-SDC4 enhances the formation of $SOX9^+/PDX1^+$ bipotent PP organoids through regulation of the SDC4-ITGAV-AKT signaling axis. This study will contribute to optimizing the source of seed cells in diabetes stem cell replacement therapy and provide a novel approach via the combination of tissue engineering and stem cell therapy for the treatment of diabetes in both basic research and clinical studies.

Methods

DIA-based proteomics analysis and verification

As outlined in our previous research, pancreatic tissues were harvested from C57/BL6 mice in the first week (Fw, $n = 3$), third week (Tw, $n = 3$), and eighth week (Ew, $n = 3$) after birth and were subjected to DIA sequencing to create a comprehensive profile of differentially expressed proteins (DEPs) during mouse pancreatic development. The procedures for protein extraction, high-pH reversed-phase fractionation, high-performance liquid chromatography–mass tandem mass spectrometry (HPLC–MS/MS) analysis and data analysis were consistent with those detailed in our earlier study [10]. To validate the results obtained from DIA analysis, the pancreatic tissues from both C57/BL6 mice and humans were fixed, embedded, and analyzed via immunofluorescence (IF) staining. This study was approved by both the Ethics Committee of the Affiliated Hospital of Nantong University and the Animal Ethics Committee of Nantong University and was conducted in accordance with the tenets of the Declaration of Helsinki.

Differentiation of SC-β cells from the hESC-H9 line

The hESC-H9 line was obtained from Professor Yan Liu of Nanjing Medical University, and the SC-β cell differentiation strategies were described in our previous article [19]. For SC-β cell differentiation, two days after passage, hESCs seeded onto 6-well plates at 3×10^5 cells/cm^2 were differentiated via an adapted 6-stage protocol. Stage 1 (5 days): definitive endoderm (DE); Stage 2 (3 days): primitive gut tube (PG); Stage 3 (3 days): posterior foregut (PFG); Stage 4 (5 days): pancreatic progenitor cells (PPs); Stage 5 (7 days): endocrine progenitors (EPs); and Stage 6 (21 days): stem cell-derived β cells (SC-β cells). The PFGs and PPs from stages 3 and 4 were transfected with shRNA; the shRNA targeting SDC4 (SDC4-shRNA) was synthesized by GenePharma Biotechnology (Suzhou, China). jetOPTIMUS (Polyplus, France) was used for shRNA transfection according to the manufacturer's protocol. The transfection efficiency was determined via IF,

quantitative real-time PCR (qRT−PCR) and flow cytometry (FCM).

Preparation of the AG73-GelMA/AlgMA hydrogel

The 5%GelMA/2%AlgMA hydrogel was prepared according to our earlier study. GelMA (EFL, China) and AlgMA (EFL, China) were dissolved in PBS with 0.25% (w/v) lithium phenyl-2,4,6-trimethylbenzoylphosphinate (LAP). This mixture was heated to 42 °C to ensure full dissolution, achieving final concentrations of 5% for GelMA and 2% for AlgMA. The prepared hydrogel mixture was then sterilized using a 0.22 μm filter and subsequently stored at -20 °C until use. The peptide AG73 (CGGGRKRLQVQLSIRTC) was biosynthesized by Sangon Biotech. For peptide grafting, AG73 was dissolved in the GelMA/AlgMA hydrogel solution with shaking for 24 h.

Characterization of the AG73-GelMA/AlgMA hydrogel

The protein structure of SDC4 was retrieved from the PDB database, and the polypeptide structure of AG73 was predicted by SWISS-MODEL software. The PDB templates for SDC4 and AG73 were uploaded to the HDOCK server for molecular docking prediction. To confirm that AG73 was successfully grafted onto the hydrogel, the hybrid hydrogel was lyophilized and ground into a powder. After being dissolved in deuterated water, the maleimide peak was detected by an AVANCE III instrument. The hydrogel equilibrium swelling ratio was determined by assessing the changes in wet weight following immersion in PBS. The initial wet weights of the appropriately sized hydrogels were recorded as W0. The weights of the hydrogels were subsequently measured at specific time points (Wt) to calculate the swelling rate via the following formula: Swelling rate = (Wt-W0/W0) × 100%. To assess the rheological behavior, the storage modulus (G′) and loss modulus (G″) were measured using an Anton Paar MCR 302 rheometer (Anton Paar Instruments, Graz, Austria). These measurements were conducted at 37 °C at a strain of 1% and utilizing a 25 mm diameter cone−plate setup. Additionally, the compression modulus of the hydrogel was determined by analyzing the stress–strain curves, which were obtained using an electronic universal material testing machine (CMT6103, MTS, USA). The curves were recorded at a deformation rate of 1 mm/minute, and the modulus was calculated from the slope of the linear portions of these curves. To investigate the microstructural characteristics of the hydrogels, the hydrogels were first lyophilized for 48 h. The microstructures of the samples were subsequently analyzed by scanning electron microscopy (SEM; Gemini 300, Zeiss, Germany). The porosity of the hydrogels was quantified by ImageJ software upon analysis of the SEM images. At least four samples from each experimental group were subjected to these tests to ensure consistent and reliable results.

hESC-H9 encapsulation and differentiation

The cell-loaded hydrogel bioink (5 million cells/mL) was encapsulated in vivo and 3D printed using a DLP printer (EFL-BP8601 series) following the methodology described in our previous study. Prior to printing, a construct with a side length of 5 mm and a chain distance of 0.4 μm was designed. Printing was performed at a UV light intensity of 10 mW/cm^2 for 60 s. A total of ten layers, each 100 μm thick, were printed. The printed constructs were subsequently transferred to culture plates and incubated in complete mTeSR™ Plus medium (100–0276, STEMCELL Technologies) for 48 h before differentiation. A four-stage protocol was employed to obtain the desired PPs. On day 5, the PPs were collected after the hydrogel was treated with collagenase, cultured, and differentiated in a 6-well ultralow adsorption culture plate. PPs, EPs and SC-β cells were encapsulated in a 2% v/v agarose gel and subjected to IF staining or transmission electron microscopy (TEM) analysis.

Hydrogel cytocompatibility

To investigate the cytocompatibility of the hybrid hydrogels, hESCs were encapsulated within the hydrogel, and CCK-8 analysis and calcein-AM/PI staining were conducted at the scheduled time points. The absorbance of each sample was measured at 450 nm with a microplate reader (MK3, Thermo Fisher Scientific, MA, United States), and the fluorescence images were observed and photographed with a Nikon Ti2-E microscope. To compare the changes in the expression of transcription factors (TFs) among the PPs cultured in different hydrogels, the hydrogels were enzymatically degraded with collagenase, and the PPs were subsequently collected for qRT−PCR analysis.

Isolation and culture of adipose-derived stem cells (ADSCs) and generation of HiPSCs

Adipose tissues were obtained from the omenta of patients who underwent partial pancreatectomy and were isolated via collagenase digestion as previously described [20]. ADSCs from P3-P5 were used to generate hiPSCs via ReproRNATM-OKSGM (STEMCELL Technologies, 05930) over approximately 20–28 days. Days 1–2: ADSCs (1×10^5 cells) were plated on Matrigel-coated 6-well plates overnight, and the growth medium was replaced the next day. The ReproRNATM Cocktail, containing ReproRNATM-OKSGM, Opti-MEM® I Reduced Serum Medium, ReproRNATM Transfection Supplement and ReproRNATM Transfection Reagent, was added to the medium for another 24 h of incubation. Days 3–6: The growth medium containing puromycin was changed

daily. Days 7–8: The growth medium without puromycin was changed daily. Days 9–15: ReproTeSRTM medium with B18R was changed daily. Days 16–28: The ReproTeSRTM medium (without B18R) was changed daily until hiPSC colonies formed. Typical hiPSC colonies were picked and passaged. To evaluate the ability of hiPSCs to form teratomas, 1×10^6 hiPSCs were resuspended in an appropriate amount of Matrigel and injected subcutaneously into NOD/SCID mice ($n = 3$). After 1 month, appropriately sized tumors were collected and histologically stained. FCM and IF were used to confirm the expression of the hiPSCs stemness marker.

mRNA sequencing (mRNA-seq) and single-cell RNA sequencing (scRNA-seq) of PP organoids

hiPSCs were encapsulated and differentiated as described in the previous sections. On day 5, mature PPs derived from the Matrigel, GelMA/AlgMA, and AG73-GelMA/AlgMA groups were collected for mRNA sequencing (mRNA-seq), whereas on day 2, immature PPs were collected for single-cell RNA sequencing (scRNA-seq). An siRNA targeting ITGAV or an AKT pathway inhibitor was introduced to the AG73-GelMA/AlgMA group during the PFG and PP stages to investigate its effect on hiPSCs differentiation into PP organoids and the underlying mechanism.

Glucose-stimulated insulin secretion (GSIS)

The SC-β cells from different groups were washed, incubated in Krebs–Ringer's solution (KRB) for 30 min, and then incubated in low-glucose (2 mM) or high-glucose (20 mM) KRB for 30 min. The insulin content in the supernatant was detected using an insulin enzyme-linked immunosorbent assay (ELISA) kit (Mercodia) and normalized to the DNA content. Single SC-β cells were dispersed with accutase (07920, STEMCELL Technologies) and counted using a cell counter (C100-SE, RWD). The same procedures were performed for cell stimulation with 30 mM KCl and 10 nm exendin-4.

Transplantation in vivo

After 12 h of fasting, 7–8-week-old nude mice were intraperitoneally administered 120 mg/kg streptozotocin (STZ) on the first and third days. Fasting blood glucose levels exceeding 16.7 mM were considered successful indicators for modeling purposes. All animal experiments conducted in this study received approval from the Animal Ethics Committee of Nantong University. SC-β cells from different groups were implanted into the subrenal capsule of type I diabetes mellitus (T1DM) mice ($n = 6$) (Fig. 5a), while diabetic mice without any intervention were used as controls. Fasting blood glucose levels were monitored by collecting blood samples from the tail vein of each mouse at various time points. Twelve weeks after transplantation, the mice were sacrificed, and the grafts were extracted for histological staining and qRT–PCR analysis. Moreover, analysis of the C-peptide and the intraperitoneal glucose tolerance test (IPGTT) were performed as we reported previously [19].

mRNA-seq

Total RNA was extracted from PPs using a Total RNA Kit (Servicebio, China). Gene Denovo Biotechnology Co., Ltd. (Guangzhou, China) constructed the complementary DNA (cDNA) libraries and performed sequencing and transcriptome data analysis. Differential expression analysis between two distinct groups was carried out using DESeq2 software. All differentially expressed genes (DEGs) were subjected to biological processes via Gene Ontology (GO) biological process and Kyoto Encyclopedia of Genes and Genomes (KEGG) pathway enrichment analyses.

scRNA-seq and data analysis

The cells were dissociated into individual cells using accutase (07920, STEMCELL Technologies) and filtered through a 40-μm cell strainer (352340, Corning). Single cells were subsequently isolated from the emulsions, and each cell was labeled with a unique set of oligonucleotides. The cDNA library was amplified via PCR. The pooled cDNA libraries from all groups were sequenced on the Illumina 10 × Genomics Chromium platform (10 × Genomics, Illumina) via paired-end reads. scRNA-seq analysis was conducted by Gene Denovo (Gene Denovo, China) following previously described methods. UMI counting and cell barcoding generated cell-by-gene matrices, which were individually imported into Seurat version 3.1.1 for cell cluster identification. Cells meeting specific criteria, such as having more than 8000 UMIs, fewer than 500 or more than 4000 genes, and a mitochondrial gene percentage greater than 10%, were excluded from further analysis. Principal component analysis (PCA) was performed to reduce dimensionality. Seurat was used to implement a graph-based clustering approach where cells were embedded in a shared nearest neighbor (SNN) graph on the basis of similar gene expression patterns. SNN graph construction involved refining edge weights between cells on the basis of common overlap and Jaccard distance calculations. Clusters were generated via the Louvain method and visualized using t-distributed stochastic neighbor embedding (t-SNE) with the same principal components used for PCA visualization.

Flow cytometry (FCM)

Cells were fixed/permeabilized for 20 min and incubated with antibodies for 30 min at 4 °C. After being washed and resuspended in PBS, the cells were detected by BD

LSRFortessa and analyzed by FlowJo v10. Detailed information regarding the antibodies used is given in table S1.

Immunofluorescence (IF)

After fixation in formaldehyde and embedding in OCT compound, the cells or tissues were sliced, and antigen retrieval was performed using sodium citrate buffer (Beyotime, China). The sections were subsequently treated with 0.5% Triton X-100 and 5% bovine serum albumin (BSA; Beyotime, China), followed by overnight incubation at 4 °C with primary antibodies. The sections were thoroughly washed the following day before being exposed to secondary antibodies and DAPI (Solarbio, China) for 1 h and 10 min, respectively. Finally, the sections were visualized and imaged under a Nikon Ti2-E microscope. Detailed information regarding the primary and secondary antibodiesused can be found in table S1.

Real-Time quantitative reverse transcription polymerase Chn reaction (qRT–PCR)

For total RNA extraction, a Total RNA Kit (Vazyme, China) was used, followed by cDNA synthesis using a First Strand cDNA Synthesis Kit (Vazyme, China). qRT–PCR analysis was conducted with SYBR Green Master Mix (Vazyme, China), and detection was performed with a QuantStudio 5 PCR system (Thermo Fisher Scientific, USA). The gene expression levels were quantified via the $2^{-\Delta\Delta Ct}$ method. The gene primers used can be found in our previous study and Table S2 [19].

Statistical analysis

The statistical analyses were performed using SPSS 22 software. The data are presented as the means ± standard deviations and were obtained from at least three independent experiments. All datasets were assessed for a normal distribution before conducting either a Student's t test or one-way ANOVA for comparisons between groups. A value of $P < 0.05$ was considered to indicate statistical significance.

Results

SDC4 affects pancreatic development and the differentiation of PPs

To investigate the involvement of the DEPs during various stages of pancreatic development in mice, we utilized hierarchical clustering analysis to examine a set of 1753 DEPs that were consistently differentially expressed across three developmental stages (for detailed information, please refer to our previous study). By employing a cluster series test, we identified eight distinct protein expression profiles. Notably, SDC4 was robustly and consistently expressed, particularly in the pancreases of the mice in the TW and EW groups (Fig. 1a). IF analysis confirmed that the expression of SDC4 in the islet tissues of the EW mice was significantly greater than that in the islet tissues of the FW and TW mice, which correlates with the location of insulin expression (Fig. 1b, c). Meanwhile, in human pancreatic specimens, SDC4 expression was detected and showed a similar spatial overlap with insulin expression (Fig. 1d). According to our previous strategies for SC-β differentiation, we downregulated cellular SDC4 at the PG and PFG stages and induce their differentiation into PPs (Fig. 1e). The FCM results revealed a significantly lower percentage of $NKX6.1^{+}/PDX1^{+}$ PPs in the SDC4-shRNA group (15.35 ± 2.659%) than in the NC group (53.26 ± 2.738%) ($P < 0.0001$) (Fig. 1g and h). This finding strongly suggests a substantial decline in the differentiation efficiency of PPs. IF and qRT−PCR revealed a significant decrease in the expression of important TFs, including PDX1, SOX9, NKX6.1, GATA4, and PAX4, in SDC4-shRNA PPs (Fig. 1h, i). mRNA analysis upon treatment with SDC4-shRNA and NC-shRNA validated the significant downregulation of these key TFs in PPs upon the loss of SDC4 (Fig. 1j). KEGG analysis revealed alterations in crucial signaling pathways involved in pancreatic endocrine cell development, including insulin secretion and pancreatic secretion, following SDC4 downregulation (Fig. 1k).

Preparation and cytocompatibility of the AG73 hydrogel

In our previous study, we successfully developed a biomimetic hydrogel composed of 5% GelMA and 2% AlgMA that possesses physiological stiffness similar to that of pancreatic tissue [11]. To reconstruct the microenvironment during pancreatic development and facilitate the cellular response to mechanical signals from the ECM, we designed the AG73 hydrogel as a platform to evaluate how AG73-SDC4-mediated signaling affects pancreatic differentiation (Fig. 2a). By conducting molecular docking simulations, we discovered that residue GLN-8 of AG73 forms hydrogen bonds with HE-13 of SDC4, indicating a binding interaction between them (Fig. 2b). We formulated AG73 hydrogels at final concentrations of 0.1 mg/mL and 1 mg/mL (Fig. 2c). The presence of the characteristic maleimide peak in the AG73 hydrogel was confirmed via nuclear magnetic resonance (NMR) analysis, indicating the successful binding of AG73 to 5%GelMA/2%AlgMA (Fig. 2d). The rheological properties of the hydrogel, including its storage modulus (G', representing elasticity) and loss modulus (G", indicating viscosity), were analyzed. The results revealed that upon exposure to UV radiation, the hybrid hydrogel exhibited improved elastic behavior and exceptional mechanical durability, with G' surpassing G" (Fig. 2e). After immersion in PBS for 48 hours, the hydrogel, low-AG73 hydrogel, and high-AG73 hydrogel exhibited swelling rates of 38.5 ± 3.4%, 40.6 ± 5.4%, and 35.5 ± 2.2%, respectively, with no significant difference between them (Fig. 2f) ($P > 0.05$).

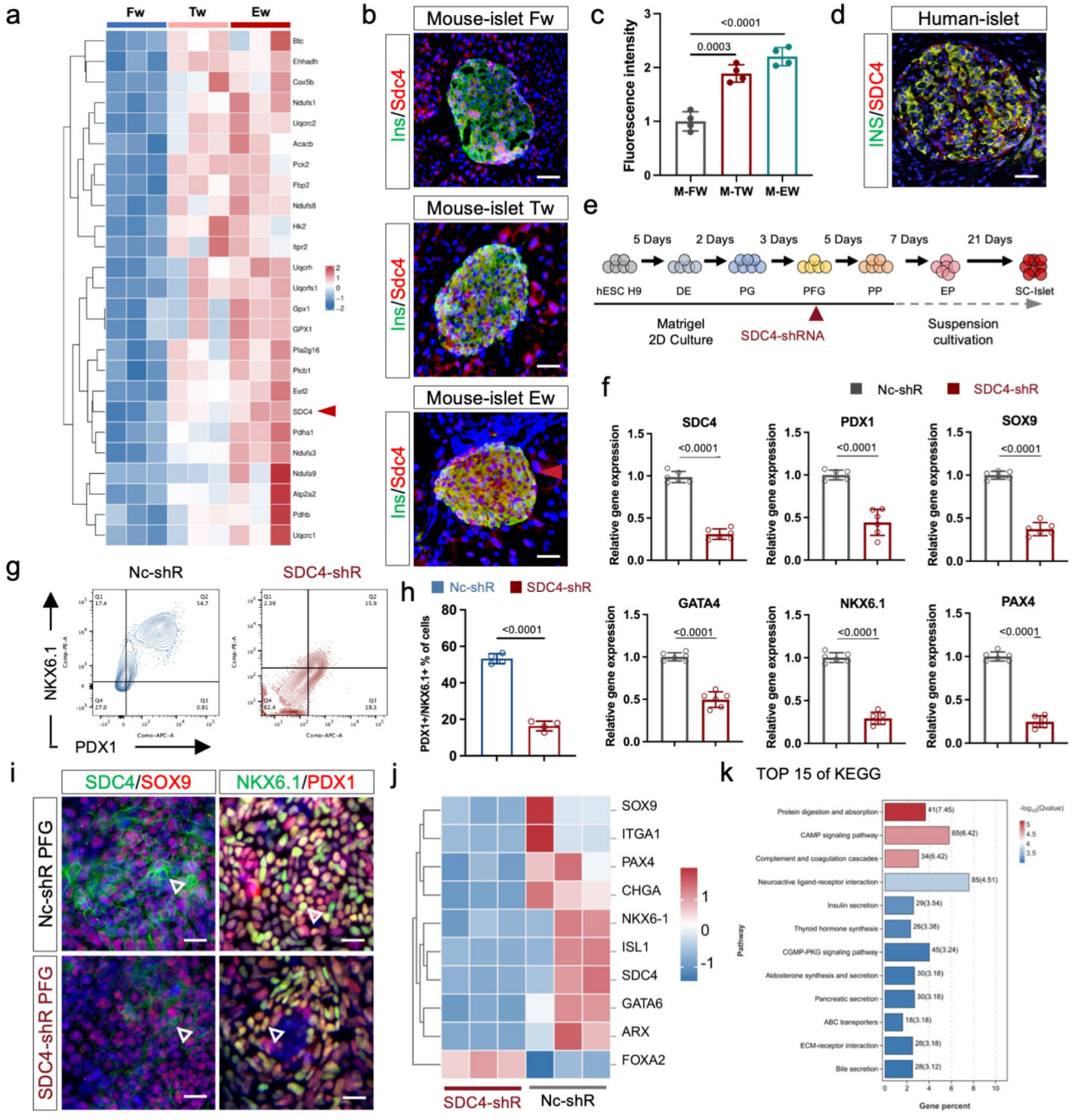

Fig. 1 Role of SDC4 in pancreatic β cell differentiation. (**a**) Schematic of DIA analysis. (**b, c**) SDC4 was highly expressed in the pancreas of mice in EW (eighth week) groups, which correlated with the expression location of insulin ($n=4$). (**e**) SDC4 expression was downregulated at the PG and PFG stages and continued to differentiate into PPs and SC-β cells. (**g, h**) FCM results revealed a significantly reduced positive rate of NKX6.1$^+$/PDX1$^+$ in PPs in SDC4-shRNA group ($n=4$) ($P<0.0001$). (**f**) qRT-PCR results revealed a significant decrease in the expression of PDX1, SOX9, NKX6.1, GATA4, and PAX4, in PPs in SDC4-shRNA group ($n=6$). (**i**) IF results revealed a significant decrease in the expression of SDC4, PDX1, and NKX6.1 in PPs in SDC4-shRNA group. (**j**) mRNA analysis validated the significant downregulation of key TFs in PPs in SDC4-shRNA group compared to NC-shRNA group ($n=3$). (**k**) KEGG analysis revealed alterations in crucial signaling pathways involved in pancreatic β cell development following downregulation of SDC4 ($n=3$)

On the basis of the stress–strain curves, the compressive moduli of the hydrogel, low-AG73 hydrogel, and high-AG73 hydrogel were 10.9 ± 1.9 kPa, 10.1 ± 1.6 kPa, and 9.0 ± 1.4 kPa on day 1 and 9.6 ± 1.6 kPa, 9.1 ± 0.9 kPa, and 8.5 ± 1.2 kPa on day 14, respectively (Fig. 2g and h) ($P>0.05$). There was no significant difference in the compressive moduli among the three hydrogels on either the first or fourteenth day. These results demonstrated that the incorporation of AG73 had no effect on the compression modulus of the hydrogel. Additionally, no significant

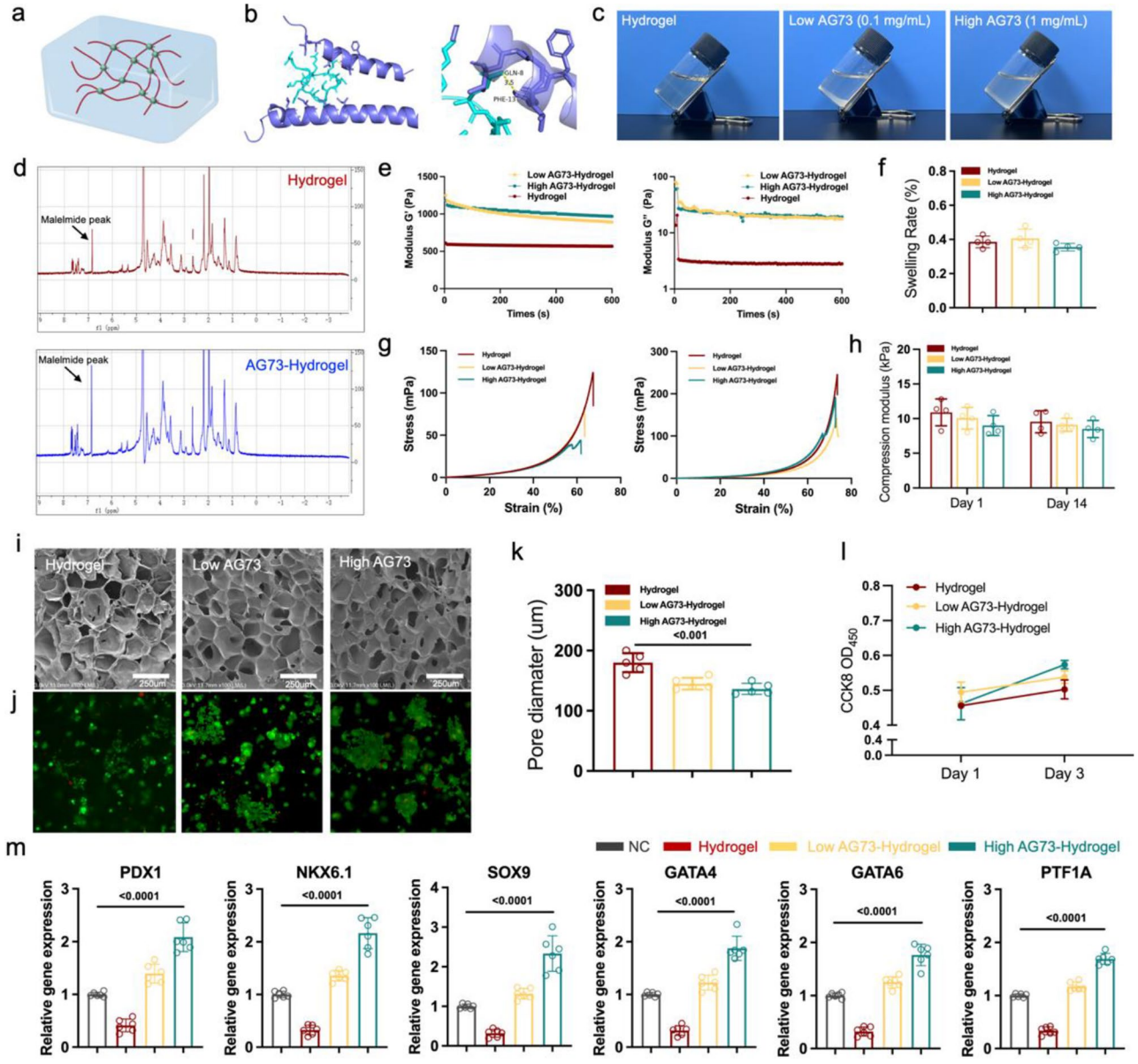

Fig. 2 Fabrication and characterization of the AG73-GelMA/AlgMA hydrogel. (**a**) Schematic diagram of AG73-GelMA/AlgMA hydrogel. (**b**) GLN-8 site of AG73 forms hydrogen bonds with the HE-13 site of SDC4. (**c**) AG73-hydrogel with final concentrations of 0.1 mg/mL and 1 mg/mL. (**d**) The characteristic Malelmide peak in AG73-hydrogel was confirmed through NMR analysis. (**e**) Rheological properties of GelMA/AlgMA hydrogel and AG73-GelMA/AlgMA hydrogel (G′ = storage modulus, G″ = loss modulus, G′ > G″). (**f**) The swelling rates of the hydrogel. (**g**) Graph of stress (kPa) varying with strain (%) of the hydrogel. (**h**) Compression modulus of the hydrogel. (**i**) SEM of the hydrogel. (**j**) Calcein-AM/PI staining showed that large numbers of dead cells were not observed in the three hydrogel groups. (**k**) Pore diameter of the hydrogel ($n = 4$) ($P < 0.001$). (**l**) The CCK-8 results at specific time points indicated no statistically significant difference in cell proliferation among the three groups of hydrogels. (**m**) High AG73 hydrogel significantly improved the efficiency of PPs differentiation compared with hydrogel alone ($n = 6$) ($P < 0.001$)

decrease in the compression modulus was observed on day 14, indicating the excellent stability of the prepared hydrogels. The SEM results revealed that the pore sizes of the three hydrogel groups were 180.0 ± 15.8 μm, 145.2 ± 9.8 μm, and 136.4 ± 9.3 μm, respectively (P < 0.001) (Fig. 2i and k). AG73 crosslinking led to a reduction in the pore size; however, the resulting pore size of the AG73 hydrogel remained within an appropriate range can provided adequate space for cellular growth. The results of calcein-AM/PI staining revealed that the hESCs' survival rate in the three hydrogel groups was satisfactory in day 3, and not many dead cells were observed (Fig. 2j). Furthermore, the CCK-8 results of hESCs proliferation in the hydrogels after 1 and 3 days were not significantly different among the three groups of hydrogels (Fig. 2l) (P > 0.05). To assess the potential of the hydrogel and

AG73 hydrogel to enhance the differentiation of hESCs into PPs, we encapsulated hESCs and subjected them to a four-stage differentiation protocol. Upon evaluation of the expression levels of the key TFs associated with PPs (PDX1, NKX6.1, SOX9, GATA4, GATA6, and PTF1A), our findings revealed that, compared with the hydrogel alone, the high-AG73 hydrogel significantly improved the differentiation efficiency of PPs (Fig. 2m).

HiPSCs generation and differentiation into PP organoids

To enhance the clinical significance of this study, we elected to utilize hiPSCs in subsequent experiments. ADSCs from P3 to P5 were selected to induce hiPSCs differentiation (Fig. 3a). After approximately 28 days of differentiation, the hiPSCs clones became visible (Fig. 3b). The FCM results revealed that a remarkable 95% of these hiPSCs were positive for NANOG/OCT4 and NANOG/SOX2 expression (Fig. S1a). Moreover, IF analysis revealed robust expression of OCT4, NANOG, SOX2 and SSEA4 (Fig. 3c). Concurrently, the hiPSCs presented positive ki67 expression, which is indicative of a robust proliferative capacity (Fig. S1b). Karyotype analysis of the chromosomes did not reveal any discernible mutations (Fig. S1c). The results of the tumor formation experiment demonstrated that subcutaneous injection of hiPSCs into nude mice induced teratoma formation, which was characterized by well-differentiated structures representing all three germ layers (the ectoderm, mesoderm, and entoderm), as revealed by histological staining (Fig. S1d).

After encapsulation into the hydrogels and differentiation into PPs, the hiPSCs formed early cellular clusters that continued to proliferate until they reached the PP stage, as observed via light microscopy (Fig. S2a). IF analysis was used to assess the differentiation efficiency of the PP organoids and revealed positive expression of the major TFs at different stages of cell differentiation, including the DE stage (FOXA2/SOX17), PFG stage (FOXA2/PDX1), and PP stage (PDX1/NKX6.1), and evaluate the effect of the AG73 hydrogel on PP organoid differentiation (Fig. 3e). The hydrogel group presented a significantly lower rate of positive TF expression. The FCM results further revealed significantly greater positive expression of PDX1/NKX6.1 in the PP organoids in the AG73 hydrogel group than in both the Matrigel group and the hydrogel group (Fig. 3f and g). Moreover, DEG analysis revealed significantly higher expression levels of key TFs (NKX6.2, PDX1, GCG, GATA6, etc.) in the PP organoids of the AG73 group than in those of the Matrigel group. Conversely, the hydrogel group presented lower expression levels of PDX1, GATA4 and NKXK6.2 than did the Matrigel group (Fig. 3i and j). KEGG pathway analysis revealed that there was enrichment of DEGs primarily in the ECM-receptor pathway, focal adhesion, the PI3K-AKT signaling pathway and the MAPK signaling pathway. GO term enrichment analysis revealed that the major enriched biological processes and molecular functions were primarily system development, tissue development, the ECM, and the development of multicellular organisms (Fig. S2c, S2d). Interestingly, we found that the PP organoids within the hydrogels exhibited a clear lumen-like structure, especially those in the AG73 group (Fig. 3e, S2b). IF revealed that epithelial markers, such as EPCAM, were significantly upregulated, indicating that the AG73 hydrogel facilitated epithelial–mesenchymal transition (EMT) in the PP organoids (Fig. 3h).

To investigate the differentiation potential of PP organoids, we extended their directed differentiation into EPs and SC-β cells (Fig. 4a). In the Matrigel group, EPs were generated via self-organization in AggreWell 400 plates, and the EPs in the AG73 group were released from the hydrogel by collagenase treatment. The EPs of the Matrigel group appeared to be more tightly packed than those of the AG73 group (Fig. 4c). However, both groups of SC-β cells eventually exhibited a tightly packed structure after 21 days culture. There was no statistically significant difference in the average diameters of EP and SC-islets between the two groups. The compact structure of AG73 hydrogel-derived SC-β was further confirmed by H&E staining (Fig. 4e). IF was used to evaluate the expression of NGN3 and YAP1 in the EPs in the Matrigel group and the AG73 hydrogel group. Our results indicated that YAP1 expression in the released EP organoids was partially translocated to the cytoplasm, suggesting a decrease in YAP activity (Fig. 4b). The findings of previous studies have demonstrated that downregulation of YAP1 expression during the late stage of PPs development promotes the differentiation of these cells into EPs [21]. Both groups of SC-β cells expressed NKX6.1, INSULIN, and MAFA (Fig. 4f). The differences in TF expression between the two groups was further analyzed via qRT−PCR and FCM. The qRT−PCR results revealed that the SC-β cells in the AG73 hydrogel group presented significantly higher expression levels of PDX1, NKX6.1, INS, MAFA, GCG and NEUROD1 than that in the Matrigel group (Fig. 4d). FCM revealed that the NKX6.1/INS and NKX6.1/MAFA positive rates in the AG73 hydrogel group were 65.5 ± 3.2% and 41.3 ± 2.1%, respectively, which were significantly greater than those in the Matrigel group (52.8 ± 3.0%, $P = 0.0011$ and 31.6 ± 2.9%, $P = 0.0015$, respectively) (Fig. 4g and h). The TEM results revealed the presence of insulin granules in the SC-β cells of both groups, suggesting that the cells had matured (Fig. 4i). SC-β cell proliferation was also compared by evaluating ki67 expression, and there was no significant difference between the SC-β cells derived from the AG73 hydrogel group and the Matrigel group. These findings suggest that both groups of cells did not excessively proliferate (Fig. 4j). In addition, glucose, KCl, and

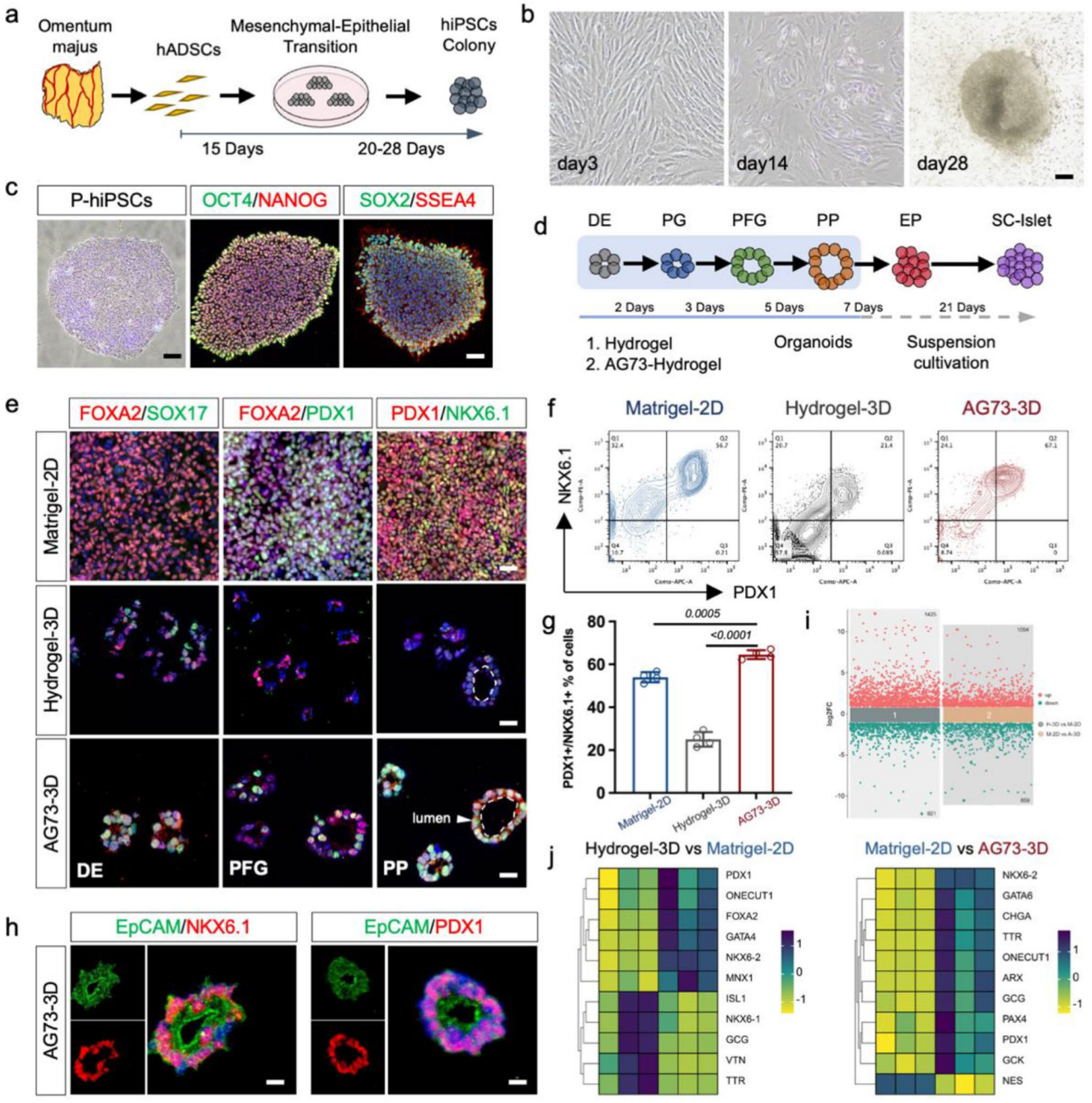

Fig. 3 hiPSCs Generation and differentiation into PP organoids. (**a**) ADSCs were induced differentiation into hiPSCs. (**b**) The formation of iPSCs clones became visible in 28 days of differentiation. (**c**) IF analysis revealed robust expression of OCT4, NANOG, SOX2 and SSEA4. (**d**) Diagram of hiPSCs differentiating into PP organoids and SC-β cells within the hydrogel. (**e**) IF analysis revealed positive expression of the major TFs at different stages of cell differentiation, including DE stage (FOXA2/SOX17), PFG stage (FOXA2/PDX1), and PP stage (PDX1/NKX6.1). (**f, g**) The FCM results demonstrated a significantly higher positive expression of PDX1/NKX6.1 in PP organoids within the AG73 hydrogel group compared to both the Matrigel group and the hydrogel group ($n=4$). (**h**) Significant upregulation of EPCAM in PP organoids in AG73 hydrogel. (**i**) Up-regulated genes and down-regulated genes in groups hydrogel group and Matrigel group, Matrigel group and AG73 group. (**j**) DEGs results revealed significantly higher expression levels of NKX6.2, PDX1, GCG, GATA6 et al. in PP organoids of the AG73 group compared to the Matrigel group. The hydrogel group exhibited lower expression levels of PDX1, GATA4 and NKXK6.2 compared to the Matrigel group

exenatide-4 were applied to the SC-β cells stimulate insulin, and significantly more insulin secretion was observed in the AG73 hydrogel group than that in the Matrigel group (Fig. 4k, l and m).

In vivo transplantation into diabetic mice

The ability of SC-β cells to regulate blood glucose levels in diabetic mice was confirmed after a 12-week transplantation experiment conducted in vivo. IF staining

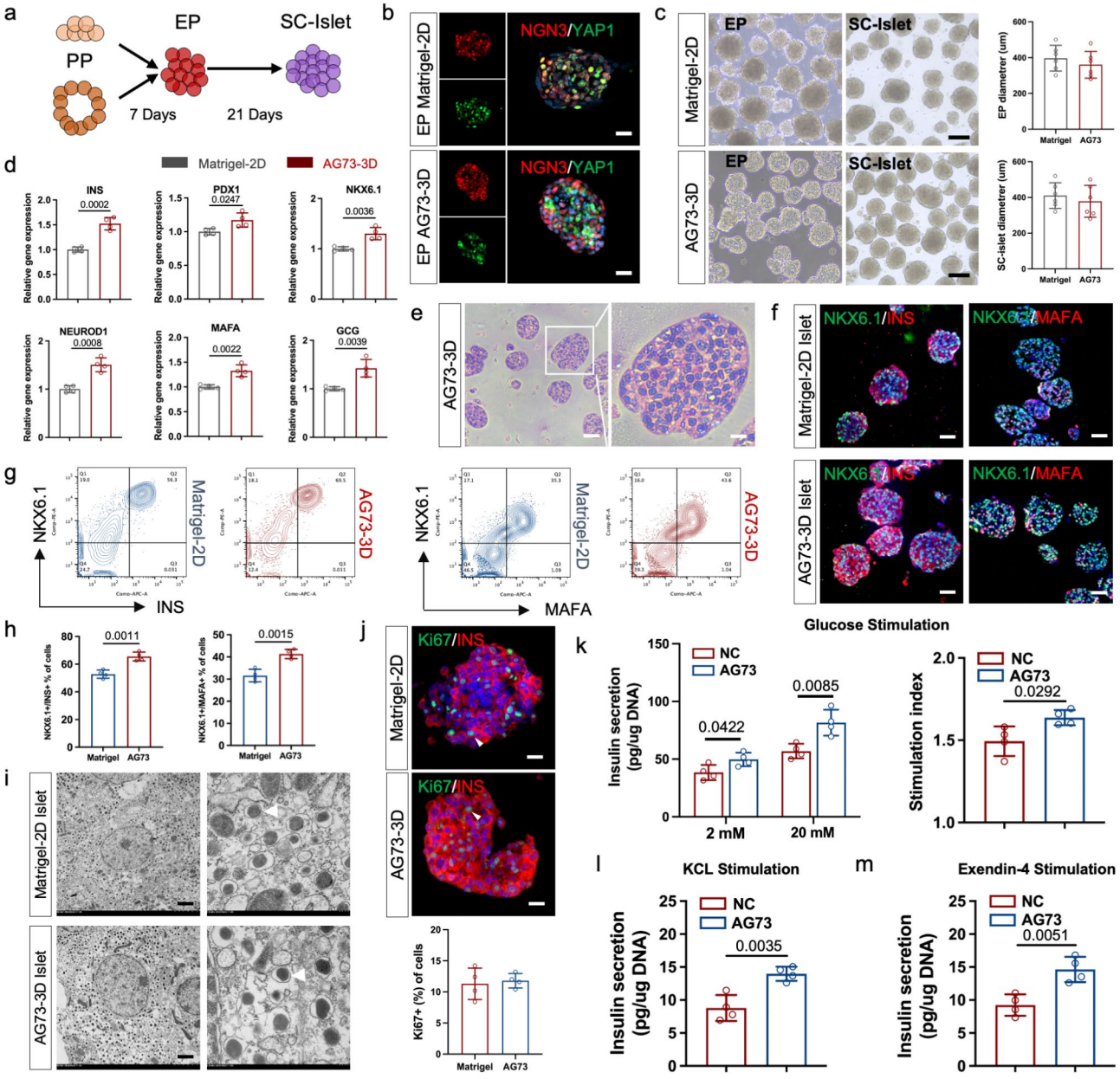

Fig. 4 PPs differentiated into EPs and SC-β cells. (**a**) PP organoids were differentiated into EPs and SC-β cells. (**b**) The expression of NGN3 and YAP1 in EPs within the Matrigel group and AG73-hydrogel group. (**c**) EPs and SC-β cells from Matrigel and AG73-hydrogel group and no statistically significant difference in their sizes. (**d**) qRT-PCR results revealed that SC-β cells in the AG73-hydrogel group exhibited significantly higher expression levels of PDX1, NKX6.1, INS, MAFA, GCG and NEUROD1 compared to the Matrigel group ($n=4$). (**e**) AG73-hydrogel derived SC-β cells exhibited a tightly packed structure. (**f**) Both groups of SC-β cells exhibited the expression of NKX6.1, INSULIN, and MAFA. (**g, h**) The positive rates of NKX6.1/INS and NKX6.1/MAFA in the AG73-hydrogel group was higher compared to those in the Matrigel group. (**i**) TEM results showed insulin granules in SC-β cells of both groups (White arrow). (**j**) ki67 expression of SC-β cells in the Matrigel and AG73-hydrogel group ($n=4$). (**k, l, m**) Insulin levels in the SC-β cells were stimulated with glucose, KCL, and exenatide-4 ($n=4$)

revealed that the differentiated SC-β cells from both groups continued to express insulin and NKX6.1 after transplantation in vivo (Fig. 5g). The positive rate of INS+/NKX6.1 + cells derived from AG73 was significantly higher compared to that in the Matrigel group ($P=0.0011$) (Fig. 5h). Moreover, serum levels of human C-peptide did not significantly differ at 1 week posttransplantation ($P>0.05$). However, there was a significantly greater disparity in the serum levels of human C-peptide between the AG73 group and the Matrigel group at 6 weeks after transplantation ($P=0.0027$) (Fig. 5b). Next, we evaluated the increase in body weight, blood glucose levels, and glucose tolerance and clearance. The observed changes in blood glucose levels within

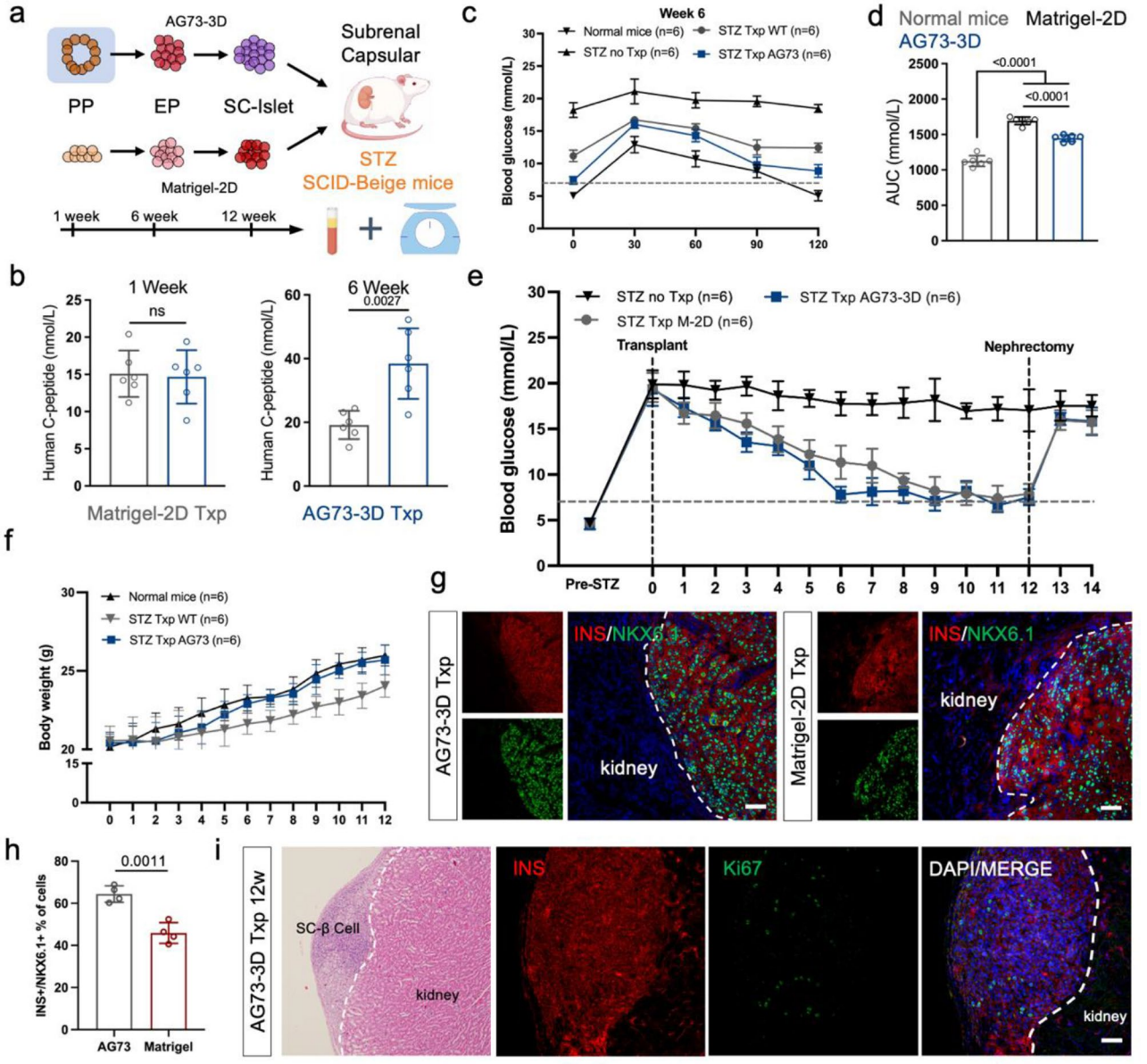

Fig. 5 SC-β cells transplantation in diabetic mice. (**a**) SC-β cells were implanted into the renal capsule of T1DM mice. (**b**) The serum levels of human C-peptide in the two groups of SC-β cells at 1 and 6 week post-transplantation. (**c, d**) The changes in blood glucose levels within 120 min after intraperitoneal glucose injection ($n=6$). (**e**) Fast blood glucose of diabetic mice engrafted with SC-β cells of different groups up to 12 weeks ($n=6$). (**f**) Mice transplanted with AG73 hydrogel derived SC-β cells demonstrated a notably higher post-transplantation increase in body weight ($n=6$). (**g, h**) Transplanted SC-β cells differentiated from the two groups continued to express insulin and NKX6.1 after transplantation in vivo and the positive rate of INS+/NKX6.1 + cells derived from AG73 was significantly higher compared to that in the Matrigel group ($n=4$) ($P=0.0011$). (**i**) IF staining of Ki67 in the transplanted area (Ki67%<1%)

120 min after intraperitoneal glucose injection indicated that diabetic mice treated with SC-β cells derived from the AG73 hydrogel exhibited significantly greater glucose tolerance and clearance than did mice in the Matrigel-treated group (Fig. 5c and d). Additionally, the body weights of the mice transplanted with SC-β cells derived from the AG73 hydrogel were notably greater than those of the mice transplanted with Matrigel at 12 weeks (Fig. 5f).

A significant difference in blood glucose levels was observed between the AG73 hydrogel group and the Matrigel group at 6 weeks after transplantation ($P<0.05$). The blood glucose levels of the AG73 hydrogel group were 6.5 ± 1.1 mmol/mL, whereas those of the Matrigel group were 11.3 ± 1.5 mmol/mL. By week 11 posttransplantation, both groups demonstrated improvements in their blood glucose levels, with measurements of 6.2 ± 0.4 mmol/mL for the AG73 hydrogel group and 6.6 ± 0.4

mmol/mL for the Matrigel group, indicating effective restoration of normal blood glucose levels. Compared with those transplanted with Matrigel, diabetic mice that received SC-β cells derived from the AG73 hydrogel presented a more rapid decrease in blood glucose levels, and this reduction ability appeared approximately 6 weeks after transplantation, as opposed to the 9 weeks required by the Matrigel group (Fig. 5e). Moreover, shortly after graft removal, both groups of recipients experienced hyperglycemia, indicating that glucose homeostasis was altered due to the transplanted SC-β cells. No significant tumor formation was observed in the kidneys 12 weeks after transplantation of SC-β cells, indicating a favorable safety profile for SC-β cell transplantation. Additionally, IF staining of Ki67 in the transplanted area revealed no evidence of excessive proliferation among the transplanted SC-β cells (Ki67%<1%) (Fig. 5i).

Single-cell transcriptome analysis of the PP organoids

To investigate how the AG73 hydrogel affects PP organoid development at the cellular cluster level, scRNA-seq was performed on day 2 of the PFG transformation into PPs. All cells were classified into 15 clusters via t-SNE analysis. The predominant clusters in the AG73 hydrogel group were clusters 1, 3, 7, 8 and 9, whereas clusters 0, 1, 4 and 6 were primarily observed in the control hydrogel group (Fig. 6a and b).

Next, we identified development-related genes expressed in PPs from both the hydrogel group and the AG73 hydrogel group. Notably, the key TFs PDX1, SOX9, NKX6.2, GATA4, GATA6 and HES1 were significantly upregulated in clusters 1, 2, and 7 (Fig. 6c). t-SNE analysis was subsequently conducted to examine the expression patterns of SOX9, GATA4, PDX1, and SDC4 as well as their distributions across different clusters. Interestingly, while PDX1, SOX9, and GATA4 were upregulated in the AG73 hydrogel group compared with the hydrogel group, the expression of SDC4 did not significantly differ between these two groups (Fig. 6d). Analysis of the entire TF subpopulation revealed that cluster 7 presented high expression levels of PDX1, SOX9, and YAP1 (Fig. 6f). The cells expressing PDX1, SOX9, and YAP1 were identified as bipotent PPs on the basis of previous studies (Fig. 6e) [22]. Subsequently, IF confirmed that PDX1 and SOX9 were expressed in the PP organoids, as both were detected in both experimental groups but they were present at higher levels in the AG73 hydrogel group (Fig. 6g, h). Cell cycle analysis revealed that there was an increase in the proportion of cells in G1 phase among the AG73 hydrogel-derived PP organoids compared with those in the hydrogel group, indicating the suppression of cell cycle progression (Fig. 6i and j). DEG analysis also revealed significant upregulation of the pancreatic endocrine factors FOXA2, SOX4, HES1, and other related genes in clusters 1 and 7 (Fig. 6k). Meanwhile, Figure S3 illustrates the marker genes for different clusters along with the KEGG analyses of cluster 0, 1, and 7. The further refined pseudotime analysis revealed a potential lineage relationship between the cells in clusters 1 and 7, suggesting that cluster 1 cells may serve as precursors for the development of cluster 7 cells (Fig. S4). Furthermore, identified significant genes that drive PP organoid differentiation via RNA profiling, the generation of rate scatter plots and characterization of the distinct kinetic behaviors for each gene (Fig. S5). The cell–cell and cell–ECM interactions in the hydrogel were further analyzed. The AG73 hydrogel-derived PP organoids presented more ligand–receptor pairs between distinct clusters, indicating enhanced intercellular communication (Fig. 7a). The HSPG signaling family, which includes SDC4, was found to be upregulated in AG73 hydrogel-derived PP organoids (Fig. 7c) [23]. Subsequent analysis revealed a significant increase in the abundance of SDC4-related receptors and ligands within the AG73 hydrogel-derived PP organoids. Additionally, substantial activation of numerous closely associated receptors, such as FN and those in the integrin family, was observed (Fig. 7b). Moreover, STRING database analysis suggested extensive links between SDC4, FN and integrins (Fig. 7d). Fibronectin contains domains that can engage both SDC4 and integrins. The expression pattern of ITGAV in both groups was further validated via t-SNE analysis, revealing that clusters 1 and 7 were significantly enriched within the AG73 hydrogel group (Fig. 7e). To validate our hypothesis, we initially conducted IF to confirm the coexpression of SDC4 and ITGAV in the PP organoids. We found that while SDC4 was expressed in both groups, the expression of ITGAV was notably greater in the AG73 hydrogel group (Fig. 7f). To further validate how ITGAV affects PP organoids development, an siRNA targeting ITGAV was introduced to the AG73 hydrogel group during the PFG and PP stages, and the culture was maintained until the PP stage was completed. IF analysis revealed a concomitant reduction in ITGAV expression, as well as diminished levels of the key TFs PDX1 and SOX9, within the PP organoids (Fig. 7g and h). Moreover, qRT–PCR analysis confirmed that the expression levels of TFs, such as PDX1, NKX6.1, SOX9, GATA4, GATA6 and PAX4 in PP organoids also decreased along with ITGAV downregulation in PP organoids (Fig. S6a). The role of AKT signaling in PP organoids differentiation was subsequently investigated by incorporating inhibitors targeting the AKT signaling pathway during the PG and PFG stages. IF analysis revealed a reduction in SOX9 and GATA4 expression within the PP organoids (Fig. 7i), supporting our findings. Additionally, qRT–PCR analysis confirmed the decreases in the expression levels of PDX1, NKX6.1, SOX9 and GATA4, following inhibition of the

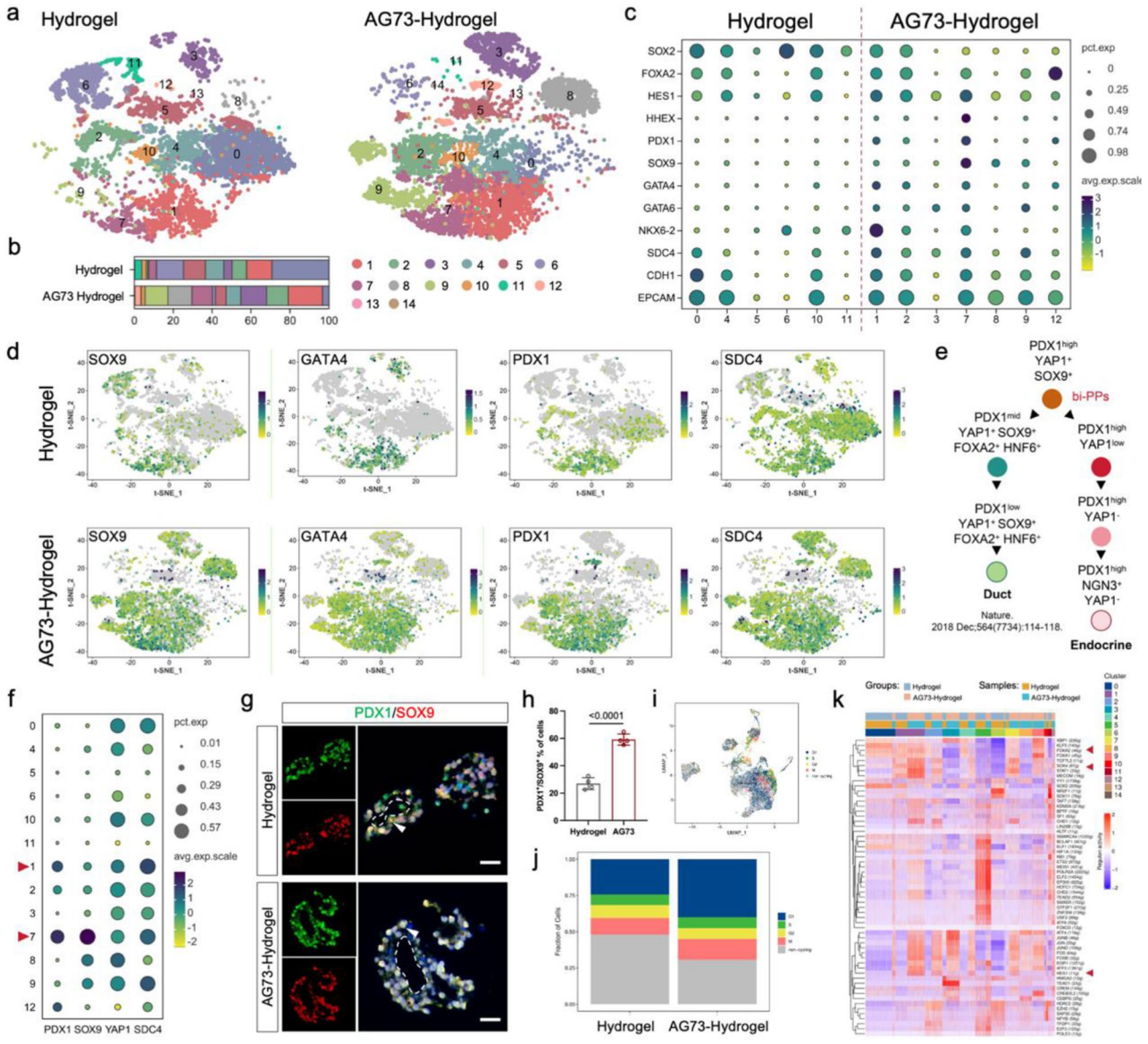

Fig. 6 Single-Cell Transcriptome Analysis of PP organoids. (**a**) PPs were classified into 15 clusters using t-SNE analysis. (**b**) The predominant clusters in the AG73 hydrogel group were clusters 1, 3, 7, 8 and 9, while clusters 0, 1, 4 and 6 were primarily observed in the control hydrogel group. (**c**) PDX1, SOX9, NKX6.2, GATA4, GATA6 and HES1 showed significant upregulation in clusters 1, 2, and 7. (**d**) The expression patterns of SOX9, GATA4, PDX1, and SDC4 as well as their distribution across different clusters. (**e**) The cells expressing PDX1, SOX9, and YAP1 were identified as bipotent pancreatic progenitors. (**f**) TFs analysis of the entire subpopulation revealed that cluster 7 exhibited high expression levels of PDX1, SOX9, and YAP1. (**g, h**) The expression of PDX1 and SOX9 in PP organoids in both groups ($n=4$). (**i, j**) The cell cycle analysis revealed an increased proportion of cells in the G1 phase for AG73 hydrogel-derived PP organoids. (**k**) DEGs analysis revealed a significant upregulation of pancreatic endocrine factors FOXA2, SOX4, HES1, and other related genes in both cluster 1 and cluster 7

AKT signaling pathway (Fig. S6b). Finally, we examined the altered adhesion properties of PP organoids in hydrogels and found that SANIL2 and N-CAD were upregulated in the AG73 hydrogel group, whereas E-CAD was downregulated. These findings suggest that the AG73 hydrogel promotes EMT in PP organoids (Fig. 7j, k).

Discussion

The development and functional maintenance of pancreatic endocrine and exocrine cells heavily rely on the intricate structure of the ECM, which not only serves as a physical and immune barrier for pancreatic cell homeostasis but also facilitates intercellular communication and matrix signaling [24]. In this study, we aimed to reconstruct the specialized proendocrine niche that is present during β-cell differentiation in vitro after identifying

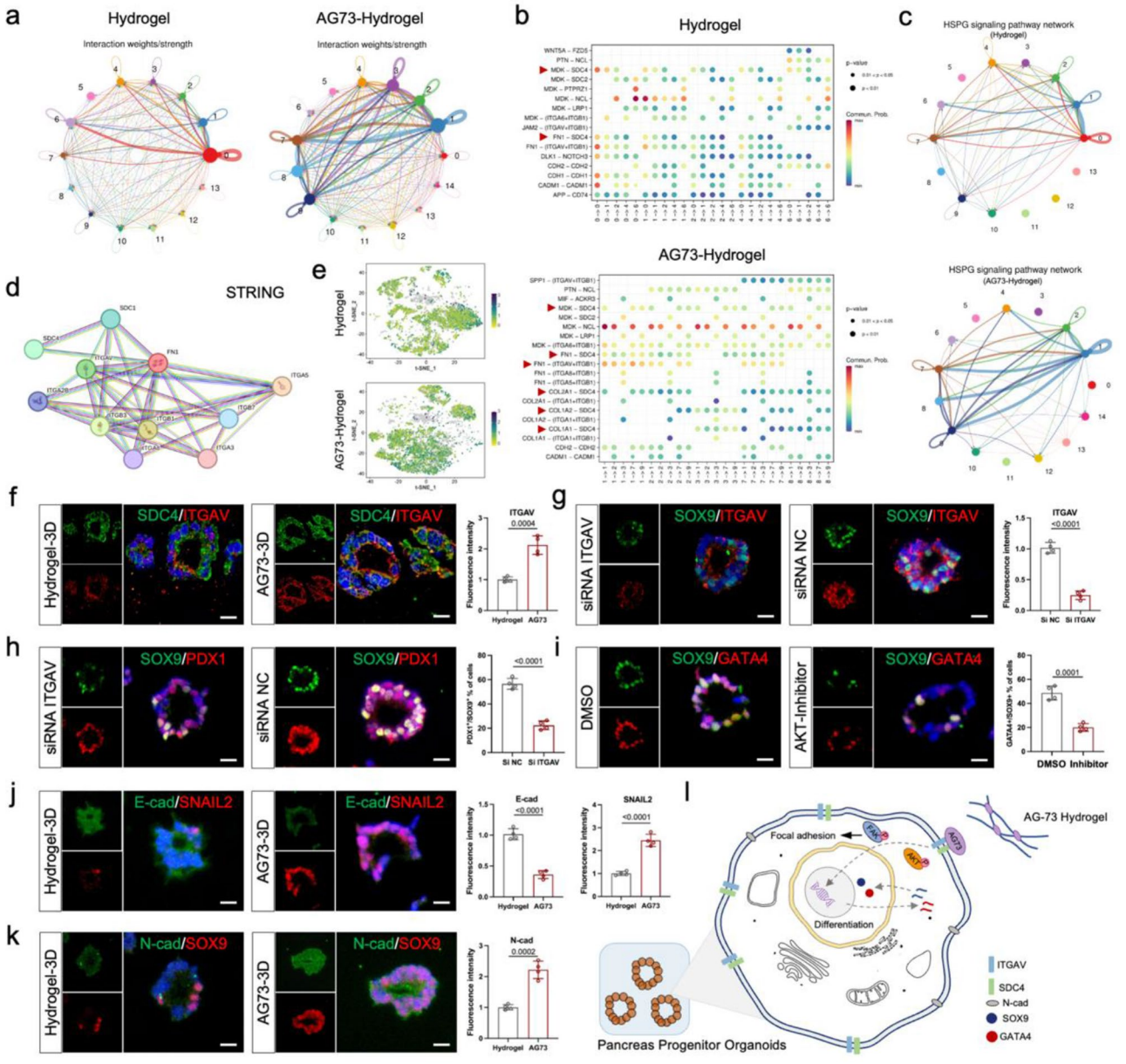

Fig. 7 Molecular mechanism of AG73 hydrogel promoting PP organoids formation. (**a**) AG73 hydrogel derived PP organoids exhibited a higher abundance of ligand-receptor pairs between distinct clusters. (**b**) Numerous receptors such as FN and the integrin family were activated observed in the AG73 hydrogel group. (**c**) The HSPG signaling family was upregulated in AG73 hydrogel-derived PP organoids. (**d**) String database suggested extensive links between SDC4, FN and integrins. (**e**) t-SNE analysis showed the expression pattern of ITGAV in the two groups. (**f**) SDC4 was expressed in both groups, the expression of ITGAV was notably stronger in the AG73 hydrogel group ($n=4$). (**g, h**) IF analysis revealed a concomitant reduction in ITGAV expression, as well as diminished levels of key TFs PDX1 and SOX9 within the PP organoids ($n=4$). (**i**) IF analysis revealed a reduction in SOX9 and GATA4 expression in PP organoids while inhibiting AKT signaling pathway ($n=4$). (**j**) E-CAD expression was downregulated and SNAIL2 expression was upregulated in the AG73 hydrogel group ($n=4$). (**k**) N-CAD expression was upregulated in the AG73 hydrogel group ($n=4$). (**l**) Molecular mechanism of AG73 hydrogel promoting PP organoids formation

SDC4 as a potential key signal transduction protein associated with pancreatic organogenesis, differentiation and maturation. On the basis of the ligand–receptor interactions between SDC4 and laminin-derived AG73, we constructed an AG73-GelMA/AlgMA hydrogel to induce the differentiation of $PDX1^{+}/NKX6.1^{+}$ PP organoids. Our research demonstrated that the AG73 hydrogel offers sufficient biomechanical support and precise biochemical signal guidance, facilitating hiPSCs differentiation into pancreatic endocrine lineages. This is in line with the findings of laminin, which, in conjunction with LAMA, facilitates the differentiation of mesenchymal cells into insulin-producing cells [25].

In this study, we used the peptide AG73 at a concentration of 1 mg/mL to mimic the physiological role of laminin in pancreatic lineage development and demonstrated its significant positive regulatory effect. In the last decade, substantial advancements have been made in the cultivation of tumor organoids utilizing the ECM, and scientists have successfully cultivated pancreatic organoids by employing Matrigel and hydrogels [26, 27]. In 2021, Alexander Kleger and Senthil K. Muthuswamy's group both published a strategy to differentiate hiPSCs into pancreatic duct-like organoids (PDLOs) [28, 29]. The hiPSCs were cultured in a 2D system for 13 days, followed by culture of $SOX9^+/PDX1^+$ PPs in a 3D environment for 17 days to generate PDLOs. These PDLOs with a duct-like morphology were subsequently utilized to establish intraductal papillary mucinous neoplasm (IPMN) organoids. Our research addresses the technical gap in obtaining PP organoids by employing 3D iPSC cultivation. Despite the widespread utilization of Matrigel and native ECM in cell and organoid culture, the unclear compositions and interbatch variability pose challenges in terms of precisely adjusting the material properties, including the mechanical and biochemical characteristics. Furthermore, the clinical translational potential of natural hydrogels is impeded by the potential for immunogenic reactions resulting from pathogen contamination [30]. To overcome the potential detrimental effects of specific components of the natural ECM on stem cell differentiation, we fabricated a hybrid hydrogel comprising GelMA with enhanced cellular bioactivity and rigid AlgMA containing hydrophilic groups for in vitro differentiation into pancreatic lineages. The application potential of GelMA/AlgMA in bone and cartilage regeneration has been demonstrated, yet there remains a dearth of systematic research pertaining to the direction of pancreatic differentiation and maturation [31]. In our previous study, a 5%GelMA/2%AlgMA hydrogel mimicking the physiological stiffness of the pancreas was confirmed to have good cytocompatibility and promote the function of insulin-producing cells. In this study, we fabricated an AG73-5%GelMA/2%AlgMA hydrogel on the basis of the receptor–ligand interaction between AG73 and SDC4, with the aim of inducing the differentiation of PP organoids. We developed a 3D culture system for hiPSC-derived PP organoids, which were maintained for up to 13 days in conventional 2D induction medium. In addition to the AG73-SDC4-guided biochemical signals, AlgMA demonstrated remarkable biological stability and chemical inertness, enabling a strategy for inducing the prolonged differentiation of PP organoids. We also compared the compressive moduli of the hydrogels on days 1 and 14, and the results revealed that there was no significant decrease.

Syndecans, as members of the transmembrane glycan protein family, can initiate transmembrane signaling pathways at the cell surface and regulate transcriptional functions within cells [32]. SDC4 has been shown to be important for PG formation [33]. Our study further revealed that SDC4 plays a pivotal role in regulating the formation of PPs during the early stages of pancreatic lineage development. 2D culture confirmed that SDC4 deficiency reduced the differentiation efficiency of $PDX1^+/NKX6.1^+$ PPs. In contrast to the GelMA/AlgMA hydrogel, the incorporation of AG73 significantly enhanced the differentiation efficiency of the $PDX1^+/NKX6.1^+$ PP organoids. Researchers are increasingly recognizing the pivotal roles mechanical signals play in governing cell fate [15]. Mechanistically, the addition of AG73 activated the SDC4/ITGAV complex and facilitated the generation of bipotent PPs expressing $SOX9^+/PDX1^+$ at the early stage of differentiation via the AKT signaling pathway. These findings demonstrated that SDC4 has the ability to activate cellular transcriptional functions by precisely discerning mechanical cues from the ECM. Studies have demonstrated that $NGN3^+$ pancreatic ductal epithelial cells are activated and migrate from the basement membrane to the pancreatic stroma during islet formation. This process involves transient EMT, which is characterized by the downregulation of E-cadherin and the upregulation of Snail2 and N-cadherin [34]. Interestingly, the addition of AG73 to PP organoids resulted in the upregulation of SNAIL and N-cad and the downregulation of E-cad. This led to a concurrent reduction in intercellular CDH1–CDH1 junctions while maintaining CDH2–CDH2 junctions. This finding is consistent with existing reports that AG73 can increase the adhesion, viability, and N-cad expression of cells encapsulated within hydrogels [14].

$SOX9^+/PDX1^+$ bipotent PPs have been recognized for their capacity to differentiate into both pancreatic endocrine and exocrine lineages. By modulating YAP1 expression, the fate of bipotent PPs can be altered, leading to distinct lineages toward the duct or endocrine system. In this study, we successfully generated PP organoids that robustly coexpressed PDX1, SOX9, and NKX6.1. A recent study demonstrated that $PDX1^+/SOX9^+/NKX6.1^+$ PPs exhibited a remarkable capacity to generate homogeneous SC islets with exceptional efficiency [35]. Further differentiation revealed that substitution of the EP induction medium in the AG73 hydrogel culture resulted in an accelerated decrease in YAP1 expression during the transition into $NGN3^+$ EPs, ultimately yielding superior SC-β cells. YAP1 has been shown to play distinct roles in pancreatic β-cells during different stages. During the PP stage, YAP1 activation maintains the proliferation and differentiation capacities of PPs; however, during subsequent differentiation, YAP1 activation attenuates the ability of PPs to further differentiate into SC-β cells,

ultimately leading to reduced efficiency [21]. Therefore, we released the organoids from the hydrogel for continued culture at the stage of PPs, as sustained ECM signaling may induce YAP1 transition activation. Our results indicated that YAP1 expression in the released EP organoids was partially translocated to the cytoplasm, suggesting a decrease in YAP activity. The nuclear import and export of YAP1 are regulated by its phosphorylation status, and future studies will aim to refine detection methods for this process. In conclusion, patient-derived PP organoids derived from ADSCs hold promise as a viable source of cells for cell replacement therapy in patients with type 1 and severe type 2 diabetes mellitus. Recently, several clinical trials have demonstrated favorable outcomes within a short timeframe using autologous insulin-producing cells derived from hiPSCs.

Conclusion

Stem cell replacement for diabetes treatment holds promise as a potential cure, yet the technical challenges of ensuring the quality, safety, and standardized production of the transplanted cells hinder its widespread clinical implementation. In the present study, the AG73 polypeptide and GelMA/AlgMA were employed to engineer hydrogels as ECM mimics, which have stable chemical properties, adjustable physical structures, and a straightforward production process. Moreover, the use of the AG73-GelMA/AlgMA hydrogel culture enables the stable and efficient formation of heterogeneous but relatively homogeneous PP organoid cells, enhances biosafety, reduces off-target effects, and decreases production costs. In future studies, we will screen additional efficacious peptides to optimize the in vitro differentiation of SC-β cells by simulating the intricate microenvironment of natural pancreatic development. Concurrently, we will leverage the reproducible and adjustable components and structures of engineered hydrogels to investigate the pivotal regulatory effects and molecular mechanisms of the ECM components and mechanical stress on pancreatic lineage development.

Supplementary Information

The online version contains supplementary material available at https://doi.org/10.1186/s12951-025-03266-5.

Supplementary Material 1

Author contributions

JW, YHL and YH conceived and designed the study. JW, YX and TMQ conducted the experiment and drafted the manuscript. XXX, YXL, MJH and YCG analyzed and interpreted the data. YH, QSG and YHL revised the manuscript. All of the authors have read, reviewed, and approved the final manuscript.

Funding

This work was financially supported by the National Key R&D Program of China (Grant Nos. 2024YFA1108200), National Natural Science Foundation of China (Grant Nos. 82372133), Science and technology project of Nantong city (Grant Nos. MSZ2022012) and Nantong Health Commission funded project (Grant Nos. MS2023021).

Data availability

No datasets were generated or analysed during the current study.

Declarations

Ethics approval and consent to participate

Experiments involving animals and human tissues were approved by the Ethics Committee of the Affiliated Hospital of Nantong University (approval number: 2024-L009) and the Animal Ethics Committee of Nantong University (approval number: S20230306-011) and was conducted in accordance with the tenets of the Declaration of Helsinki.

Consent for publication

Written informed consent for publication was obtained from all participants.

Competing interests

The authors declare no competing interests.

Author details

[1]Department of Hepatobiliary and Pancreatic Surgery, Affiliated Hospital of Nantong University, Medical School of Nantong University, Nantong, China
[2]Research Center of Clinical Medicine, Affiliated Hospital of Nantong University, Medical School of Nantong University, Nantong, China
[3]Key Laboratory of Neuroregeneration of Jiangsu and Ministry of Education, NMPA Key Laboratory for Research and Evaluation of Tissue Engineering Technology Products, Co- Innovation Center of Neuroregeneration, Nantong University, Nantong, China
[4]Medical School of Nantong University, Nantong, China
[5]Department of Nephrology, Rugao Hospital of Traditional Chinese Medicine, Nantong, China

Received: 6 November 2024 / Accepted: 21 February 2025
Published online: 27 February 2025

References

1. Shapiro AM, Pokrywczynska M, Ricordi C. Clinical pancreatic islet transplantation. Nat Rev Endocrinol. 2017;13(5):268–77.
2. Wang S, Du Y, Zhang B, Meng G, Liu Z, Liew SY, et al. Transplantation of chemically induced pluripotent stem-cell-derived Islets under abdominal anterior rectus sheath in a type 1 diabetes patient. Cell; 2024.
3. Hogrebe NJ, Ishahak M, Millman JR. Developments in stem cell-derived islet replacement therapy for treating type 1 diabetes. Cell Stem Cell. 2023;30(5):530–48.
4. Melton D. The promise of stem cell-derived islet replacement therapy. Diabetologia. 2021;64(5):1030–6.
5. Ma X, Lu Y, Zhou Z, Li Q, Chen X, Wang W, et al. Human expandable pancreatic progenitor-derived B cells ameliorate diabetes. Sci Adv. 2022;8(8):eabk1826.
6. Nostro MC, Sarangi F, Yang C, Holland A, Elefanty AG, Stanley EG, et al. Efficient generation of NKX6-1 + pancreatic progenitors from multiple human pluripotent stem cell lines. Stem Cell Rep. 2015;4(4):591–604.
7. Kozlowski MT, Crook CJ, Ku HT. Towards organoid culture without matrigel. Commun Biol. 2021;4(1):1387.
8. Ma H, Xu L, Wu S, Wang S, Li J, Ai S, et al. Supragel-mediated efficient generation of pancreatic progenitor clusters and functional glucose-responsive islet-like clusters. Bioact Mater. 2024;41:1–14.
9. Yang YH, Khan Z, Ma C, Lim HJ, Smith Callahan LA. Optimization of adhesive conditions for neural differentiation of murine embryonic stem cells using hydrogels functionalized with continuous Ile-Lys-Val-Ala-Val concentration gradients. Acta Biomater. 2015;21:55–62.

10. Huang Y, Xu Y, Zhu J, Wan J, Xiong Y, Jiang Z, et al. An artificial LAMA2-GelMA hydrogel microenvironment for the development of pancreatic endocrine progenitors. Biomaterials. 2022;291:121882.
11. Zhu S, Xu Y, Li Y, Wang L, Huang Y, Wan J. Biomimetic hydrogels promote pseudoislet formation to improve glycemic control in diabetic mice. ACS Biomater Sci Eng. 2024;10(4):2486–97.
12. De Belly H, Paluch EK, Chalut KJ. Interplay between mechanics and signalling in regulating cell fate. Nat Rev Mol Cell Biol. 2022;23(7):465–80.
13. Chronopoulos A, Thorpe SD, Cortes E, Lachowski D, Rice AJ, Mykuliak VV, et al. Syndecan-4 tunes cell mechanics by activating the kindlin-integrin-RhoA pathway. Nat Mater. 2020;19(6):669–78.
14. Tan X, Jain E, Barcellona MN, Morris E, Neal S, Gupta MC, et al. Integrin and syndecan binding peptide-conjugated alginate hydrogel for modulation of nucleus pulposus cell phenotype. Biomaterials. 2021;277:121113.
15. Yi SA, Zhang Y, Rathnam C, Pongkulapa T, Lee KB. Bioengineering approaches for the advanced organoid research. Adv Mater. 2021;33(45):e2007949.
16. Gan Z, Qin X, Liu H, Liu J, Qin J. Recent advances in defined hydrogels in organoid research. Bioact Mater. 2023;28:386–401.
17. Majumder J, Torr EE, Aisenbrey EA, Lebakken CS, Favreau PF, Richards WD, et al. Human induced pluripotent stem cell-derived planar neural organoids assembled on synthetic hydrogels. J Tissue Eng. 2024;15:20417314241230633.
18. Jiang L, Shen Y, Liu Y, Zhang L, Jiang W. Making human pancreatic islet organoids: progresses on the cell origins, biomaterials and three-dimensional technologies. Theranostics. 2022;12(4):1537–56.
19. Xu Y, Mao S, Fan H, Wan J, Wang L, Zhang M, et al. LINC MIR503HG controls SC-β cell differentiation and insulin production by targeting CDH1 and HES1. Adv Sci (Weinh). 2024;11(13):e2305631.
20. Wan J, Wu T, Wang K, Xia K, Yin L, Chen C. Polydopamine-modified decellularized intestinal scaffolds loaded with adipose-derived stem cells promote intestinal regeneration. J Mater Chem B. 2022;11(1):154–68.
21. Rosado-Olivieri EA, Anderson K, Kenty JH, Melton DA. YAP Inhibition enhances the differentiation of functional stem cell-derived insulin-producing B cells. Nat Commun. 2019;10(1):1464.
22. Mamidi A, Prawiro C, Seymour PA, de Lichtenberg KH, Jackson A, Serup P, et al. Mechanosignalling via integrins directs fate decisions of pancreatic progenitors. Nature. 2018;564(7734):114–8.
23. Chen Z, Lv Z, Zhuang Y, Saiding Q, Yang W, Xiong W, et al. Mechanical Signal-Tailored hydrogel microspheres recruit and train stem cells for precise differentiation. Adv Mater. 2023;35(40):e2300180.
24. Li Z, Tremmel DM, Ma F, Yu Q, Ma M, Delafield DG, et al. Proteome-wide and matrisome-specific alterations during human pancreas development and maturation. Nat Commun. 2021;12(1):1020.
25. Lin HY, Tsai CC, Chen LL, Chiou SH, Wang YJ, Hung SC. Fibronectin and laminin promote differentiation of human mesenchymal stem cells into insulin producing cells through activating Akt and ERK. J Biomed Sci. 2010;17(1):56.
26. Broutier L, Andersson-Rolf A, Hindley CJ, Boj SF, Clevers H, Koo BK, et al. Culture and establishment of self-renewing human and mouse adult liver and pancreas 3D organoids and their genetic manipulation. Nat Protoc. 2016;11(9):1724–43.
27. Boj SF, Hwang CI, Baker LA, Chio II, Engle DD, Corbo V, et al. Organoid models of human and mouse ductal pancreatic cancer. Cell. 2015;160(1–2):324–38.
28. Breunig M, Merkle J, Wagner M, Melzer MK, Barth TFE, Engleitner T, et al. Modeling plasticity and dysplasia of pancreatic ductal organoids derived from human pluripotent stem cells. Cell Stem Cell. 2021;28(6):1105–e11241119.
29. Huang L, Desai R, Conrad DN, Leite NC, Akshinthala D, Lim CM, et al. Commitment and oncogene-induced plasticity of human stem cell-derived pancreatic acinar and ductal organoids. Cell Stem Cell. 2021;28(6):1090–e11041096.
30. Soliman BG, Nguyen AK, Gooding JJ, Kilian KA. Advancing synthetic hydrogels through Nature-Inspired materials chemistry. Adv Mater 2024: e2404235.
31. Zhang Y, Li D, Liu Y, Peng L, Lu D, Wang P, et al. 3D-bioprinted anisotropic bicellular living hydrogels boost osteochondral regeneration via reconstruction of cartilage-bone interface. Innov (Camb). 2024;5(1):100542.
32. Afratis NA, Nikitovic D, Multhaupt HA, Theocharis AD, Couchman JR, Karamanos NK. Syndecans - key regulators of cell signaling and biological functions. Febs J. 2017;284(1):27–41.
33. Bergmann S, Penfold CA, Slatery E, Siriwardena D, Drummer C, Clark S, et al. Spatial profiling of early primate gastrulation in utero. Nature. 2022;609(7925):136–43.
34. Rukstalis JM, Habener JF. Snail2, a mediator of epithelial-mesenchymal transitions, expressed in progenitor cells of the developing endocrine pancreas. Gene Expr Patterns. 2007;7(4):471–9.
35. Jarc L, Bandral M, Zanfrini E, Lesche M, Kufrin V, Sendra R et al. Regulation of multiple signaling pathways promotes the consistent expansion of human pancreatic progenitors in defined conditions. Elife 2024, 12.

Publisher's note